J. Coates-Marnane, J. Olley, J. Tibby, J. Burton, D. Haynes, J. Kemp
A 1500 year record of river discharge inferred from fluvial-marine sediments in the Australian subtropics
Palaeogeography, Palaeoclimatology, Palaeoecology, 2018; 504:136-149

Published at: http://dx.doi.org/10.1016/j.palaeo.2018.05.019

A 1500 year record of river discharge inferred from fluvial-marine sediments in the Australian subtropics

Coates-Marnane, J[1*], Olley J[1], Tibby J[2], Burton J[3], D. Haynes[4], Kemp J[1]

[1]Australian Rivers Institute, Griffith University, Nathan, QLD 4111, Australia

[2]Department of Geography, Environment and Population and Sprigg Geobiology Centre, The University of Adelaide, SA 5005, Australia

[3]Chemistry Centre, Department of Environment and Science, Dutton Park, QLD 4102, Australia

[4]Department of Earth Sciences, School of Physical Sciences Sprigg Geobiology Centre, The University of Adelaide, SA 5005, Australia

*Corresponding author: j.coatesmarnane@griffith.edu.au

Abstract

In Australia, there is a scarcity of high resolution hyrdoclimate reconstructions for the last several millennia. Fluvial-marine sediments offer a potential avenue for examining trends in freshwater input to coastal settings and, by inference, past hydroclimates. Here, major elemental geochemistry, $\delta^{13}C$ and C:N ratios of organic matter, grain size and diatom species abundance, measured in a 4.4 m long sediment core collected from Moreton Bay, in east coast Australia, are used to infer the relative freshwater discharge of the adjacent catchment over the last ~1500 years. Reduced freshwater discharge into the Bay occurred from 630 to 1200 CE, especially between 1100 and 1200 CE. A broad increase in discharge is indicated after 1300 CE, extending to the present. The initial shift to the prolonged wet period coincides with both a decrease in the frequency of 'dry' El Niño events based on regional records from the austral Pacific, and a broad hemispheric-scale cooling trend. This record provides further insight into low amplitude climate variability in the Australian subtropics over the last 1000 years, supporting efforts in both forecasting current and future climates, and managing regional water resources. Importantly, instrumental records do not cover the full range of natural climate variability experienced in the region over the last 1000 years.

1. Introduction

The Australian subtropics are one of the most hydrologically variable regions of the continent (Rustomji et al., 2009). Variations in rainfall and river flow in these regions are strongly linked to major teleconnections such as the El Niño Southern Oscillation (ENSO) and the Pacific Decadal Oscillation (PDO) (Kiem and Verdon-Kidd, 2012; Rodriguez-Ramirez et al., 2014). At the beginning of the 21st century, much of the region experienced one of the most severe droughts on the instrumental record, the millennium drought. This was followed from 2009-2013 by a wet phase, associated with the 2010/2011 La Niña, one of the strongest events recorded in Australia, and which resulted in widespread flooding of coastal rivers including our study catchment (Cai and van Rensch, 2012). Placing such oscillations in a broader temporal context is difficult because in Australia there is a lack of well resolved

(i.e. annual-decadal) climate reconstructions for the last millennia, with arguably greater focus on temperature reconstructions than hydroclimate (Gergis et al., 2016; PAGES 2k Consortium, 2013). Continuous rainfall and streamflow monitoring only began in Australia in the early 1800s. This limits our understanding of long term climate variability and the relative importance of major atmospheric and oceanic climate systems.

In January 2011 rainfall associated with the 2010/2011 La Niña resulted in severe flooding within the Brisbane River catchment, south-east Queensland. Extensive floodplain inundation particularly within the Lockyer Valley and Brisbane City resulted in significant damage to infrastructure. The 2011 flood was one of the largest of the historical record, with a peak discharge of ~12,400 m^3 s^{-1} (Kemp et al., 2015). High stream discharges over an extended wet season resulted in severe erosion of river banks (Grove et al., 2013; Thompson et al., 2013; McMahon et al., 2017), and the deposition of extensive muddy deposits in Moreton Bay, the receiving waters of the Brisbane River (Lockington et al., 2017). The severity of this flood has promoted ongoing research into improving the understanding of the frequency of extreme floods in the region (Croke et al., 2016), their geomorphic impacts (Thompson and Croke, 2013; Kemp et al., 2015), and how such events relate to oscillations in climate (Haines and Olley, 2017; Lam et al., 2017).

As the Earth's climate warms, strong La Niña and El Niño events are predicted to increase in frequency (Cai et al., 2014, 2015). These changes are likely to contribute to an increasing occurrence of severe droughts and floods (Power et al., 2017). However, accurately forecasting the impacts of future climatic changes on water resources for individual regions can be problematic in the absence of an understanding of the full range of natural variability. Limited work has focused on resolving annual to decadal climatic trends of the more recent past (last 2,000 years) throughout a range of climatic zones across the continent (Cook et al., 2000, Yan et al., 2011; Barr et al., 2014; Haig et al., 2014). This can be credited in part to the limited geographic extent of palaeo-archives that lend themselves to high resolution inquiry (e.g. varved lake sediments, speleothems, long-lived trees and coral skeletons). In the few instances where high resolution records of climate have been developed, these have either been

restricted to temperate (Saunders et al., 2012; Barr et al., 2014) or tropical (Haig et al., 2014; Lough et al., 2015) climatic zones, or based on atmospheric teleconnections (Vance et al., 2015), which can be problematic given these connections are unstable through time (Gallant et al. 2013). This limits our understating of natural climate variability in the Australian subtropics. Fluvial-marine settings, actively accreting Holocene-aged sediment, may offer new records of past climates.

1.1 Fluvial-marine sediments as archives of climate

Sheltered estuarine embayments that receive sediment often preserve thick sequences of Holocene-aged sediments (Lamb et al., 2006; Zong et al., 2006; Clement et al., 2017). These fluvial-marine sedimentary environments are subject to both ocean processes (i.e. waves, currents, sea level variation) and riverine processes (i.e. river discharge, sediment load). High sedimentation rates also mean these environments are capable of recording relatively high frequency events including floods and storms. As a marginal environment where the deposition of both terrigenous and marine biological and mineral sediments occurs, proxies developed from fluvial marine sediments can offer insights into past fluvial and oceanic process and by inference, past climate (Zong et al., 2006; De Dekker et al., 2014; Hanna et al., 2018). However, due to the dynamic nature of sediment reworking and transport within these settings, records may be interrupted by temporal hiatuses (Yi et al., 2003).

Estuaries are ecotones that mark the transition between riverine and marine ecosystems (Roy et al., 2001). Estuaries also support a wide range of organisms, many of which are sensitive to salinity and can be well preserved in sediments. Diatoms are a diverse group of organisms that occur in a range of aquatic environments; including fresh, brackish and marine waters. Detailed investigation of diatom assemblages in freshwater and estuarine systems has shown that sensitivity to variations in water quality parameters such as pH, total phosphorus, temperature, salinity and water clarity are diverse and often species specific (Tibby and Reid, 2004; Grinham, 2011; Tibby and Taffs, 2011). This diversity and strong sensitivity to environmental fluctuations allows diatoms to be used to reconstruct climate-driven disturbances preserved in estuarine, coastal and shelf sediments (Owen et al., 1998; Zong et al., 2006;

Taylor and McMinn, 2001). In proxy-use, these microfossils are ideally paired with biogeochemical indicators (i.e. $\delta^{13}C$, C/N, mineral ratios, grain size etc.) to further refine palaeoenvironmental shifts inferred from fossil assemblages.

Organic matter in estuaries is derived from a mixture of allochthonous terrigenous and marine, and autochthonous estuarine sources. An effective means of differentiating marine plants (i.e. macro-algae, phytoplankton, and seagrass), from terrestrial plants is by using $\delta^{13}C$ values and C/N ratios of plant material (Fry et al., 1977). The $\delta^{13}C$ ratios for terrestrial plants typically range from -13 ‰ to -30 ‰, with C3 plants ranging between -23 ‰ and -30 ‰, and C4 plants (i.e. some grasses) averaging around -13 ‰ (Emery et al., 1967; Fry et al., 1977). Terrestrial plants also have high C/N ratios (typically > 12), due to the presence of cellulose and lignin, which are poor in nitrogen (Emery et al., 1967). Marine algae and plants have higher $\delta^{13}C$ values, ranging from -10 to -20 ‰ and much lower C/N ratios, typically between 4 and 10 (Bird et al., 1995; Cloern et al., 2002). $\delta^{13}C$ and C/N ratios of bottom sediments are typically between end-member values for marine and freshwater environments, which is a reflection of the relative proportion of carbon in sediment derived from distinct terrestrial and marine plant groups (Fontugne and Jouanneau, 1987; Thornton and McManus, 1994). Sheltered embayments also receive terrigenous mineral sediments in the form of clay, silt and sand from rivers. In addition to these allochthonous sediments, autochthonous sediments are produced in the form of calcium carbonates and biogenic silica derived from marine organisms; including diatoms, sponges, foraminiferans and molluscs. The relative contribution of terrestrial sediments and marine sediments may also provide evidence for the relative influence of these distinct sources in estuarine mixing zones.

In this study, diatom species relative abundance, $\delta^{13}C$ and C/N ratios (weight basis) of organic matter, grain size, and major elemental geochemistry were measured in a sediment core collected from pro-delta sediments within a shallow protected bay. Shifts in sediment composition observed in response to the 2011 flood were used as a reference for identifying periods of past increased freshwater flow discharge. An index of freshwater discharge to the bay was then constructed based on the combined proxy signals measured in the sediment core, covering the last 1500 yrs.

2. Regional setting

Moreton Bay is a semi-enclosed subtropical estuarine embayment situated adjacent to the city of Brisbane in south-east Queensland, Australia (Fig. 1). The bay is shallow, with an average depth of 7 m. To its east, the bay is bordered by two dune-barrier islands (Moreton Island and North Stradbroke Island), which act to confine bay waters and limit oceanic mixing (Dennison and Abal, 1999). A strong water quality gradient exists in the bay grading from turbid, brackish water in the west to clear, oceanic water in the east (Dennison and Abal, 1999). Moreton Bay's catchment consists of four major river systems (Brisbane, Logan, Pine, and Caboolture Rivers) with the Brisbane River catchment being the largest (13,100 km^2). The watershed of Moreton Bay has experienced significant alteration following European settlement, beginning in the 1840s, when the introduction of European livestock initiated fundamental changes in catchment dynamics, later followed by clearing of native forest, cropping and the expansion of suburban residential land (Kemp et al., 2015; 2018).

Broadly, the geology of the catchment of Moreton Bay is characterized by Mesozoic sedimentary rocks, including both Triassic and Jurassic sequences of sandstone and siltstone, with minor rhyolite and tuff. In the upper parts of the catchment, Tertiary basalts are also important, comprising major sections of the Great Dividing Range (Day et al., 1983). Within the Bay itself, Tertiary basalts and laterites form prominent coastal outcrops, while Holocene-aged fluvial-marine sediments form much of the coastal plain and modern coastline. The protection of this coastline from the open ocean has allowed for the development of a prominent fluvially-dominated delta at the mouth of the Brisbane River. The distribution of these Holocene sedimentary units within Moreton Bay has largely been controlled by the nature of sea level transgression and stabilization following the Last Glacial Maximum (Evans et al., 1992; Lewis et al., 2008). Western subtidal regions of the bay are comprised of fluvial deltaic sands with pro-delta muds extending eastward into the marine basin (Evans et al., 1992). Within the central bay area, Holocene pro-delta muds are ~10 m thick (Evans et al., 1992). High sedimentation rates of pro-delta muds in this setting provide potential for the development of high resolution palaeo records (Coates-Marnane et al., 2016). Postglacial sea level reached its highest point

in southern Queensland at ~7000 years BP with a height of ~ +1.0 – 1.5 m (AHD). Sea level then stabilized to its present position by ~2000 years BP (Lewis et al., 2008).

The region is subtropical with predominantly summer rainfall. Mean annual rainfall throughout the 21,220 km^2 catchment varies from 800 to 1200 mm, generally increasing toward the coast. The majority of summer rainfall is produced by the convection of onshore trade winds, with widespread rainfall also occurring in association with east coast troughs and storm cells. ENSO is the dominant driver of regional inter-annual rainfall variability (Chiew et al., 1998; Risbey et al., 2009), and is also modulated by longer term climate oscillations including the Pacific Decadal Oscillation (PDO) and the Interdecadal Pacific Oscillation (IPO) (Power et al; 2006; Rodriguez-Ramirez et al., 2014). The interactions of these climate phenomena results in multi-decadal wet and dry cycles observed in the instrumental record (Haines and Olley, 2017). Variability in annual rainfall is also strongly influenced by the activity of tropical cyclones and tropical low pressure systems which can propagate southward and bring sustained, intense rainfall to the region (Power and Callahan, 2016). In the east Australian tropics and subtropics the La Niña phase of ENSO is manifest as an increased likelihood of above average annual rainfall and flooding (Ramsay et al., 2012; Ward et al., 2014).

3. Methods

3.1 Bay-wide sediment survey

In November 2013 subtidal sediments were collected using a Van Veen grab sampler from 37 sites within Moreton Bay and the estuarine reach of the lower Brisbane River (Fig. 1). The sampling range spanned the estuarine mixing zone from the limit of tidal influence in the lower Brisbane River to the oceanic waters of central and eastern Moreton Bay. Sites were selected based on locations of previous water quality monitoring within the region which includes monthly measurements of salinity, turbidity, secchi depth, and pH as part of the Ecosystem Health Monitoring program (EHMP, 2011). Most sites sampled consisted of bioturbated muds, with three sites in the western bay region located in

sandy calcareous sediments. Sediments were stored at 4 ºC until they could be prepared for analysis of $\delta^{13}C$ and C/N ratios by isotope ratio mass spectrometry (IRMS).

Sediments were first dried at 60 ºC, and ground using a zirconium shatter box grinder to achieve textural consistency before analysis. For $\delta^{13}C$, samples were pre-treated with dilute (10 %) hydrochloric acid to remove inorganic carbon ($CaCO_3$), and dried at 60 C˚ for 48 hours. Then 80 mg of material was weighed and pelletized in silver capsules. Samples were combusted in a Sercon Europa elemental analyser with sample gases delivered to a Sercon Hydra IRMS at the Australian Rivers Institute, Griffith University. Results are expressed as the permil (‰) difference in isotope ratio relative to Pee Dee Belemnite ($\delta^{13}C$). The precision of $\delta^{13}C$ (‰) was monitored with a sucrose standard over 20 runs, reporting $\delta^{13}C$ = -11.7 ‰ (SD = 0.005, N = 84).

3.2 Sediment core sampling

In November 2011 a sediment core was collected from pro-deltaic sediments of the Central bay. A 4.4 m long sediment core (referred to from here as MB1L) was extracted using a purpose-built barge mounted hydraulic vibracorer designed to sample subtidal sediment profiles. On extraction, the core, sampled using steel coring barrels, was then extruded into soft black plastic tubing to preserve the luminescence properties of the sediment and stored at 4ºC until sectioning. In addition, a short core was taken from the less well-consolidated surficial sediments, positioned within 1 m of the long core (referred to from here as MB1S). This was done to ensure the recovery of the complete sediment profile that may not have been achieved using the vibra-corer alone. Divers using SCUBA, hammered a 1500 mm diameter PVC pipe into the sediment and used suction to retrieve a section of sediment (55 cm).

3.3 Geochronology

The chronology of sediment deposition was determined using a combination of fallout radionuclides (^{137}Cs and ^{210}Pb), optically stimulated luminescence (OSL) and accelerated mass

spectrometry radiocarbon (AMS ^{14}C) dating. Full details of the dating techniques and results are given in Coates-Marnane et al. (2016). In brief, four samples were taken for OSL burial age determination (50-55 cm, 100-105 cm, 351-356 cm, 439-444 cm). Single aliquot regeneration was performed with quartz sands (63 – 125 µm) on Riso instrumentation using the protocol outlined in Olley *et al.*, (2004). Single aliquot equivalent doses (D_e) were used to determine the burial dose (D_b) using the age modelling approach of Galbraith and co-workers (Galbraith et al., 1999). The dose rates (D_r) were determined by high resolution gamma spectrometry of sediments adjacent to the OSL samples in the core profile, accounting for β-attenuation factors, cosmic and internal alpha doses. The burial age was then calculated as D_b/D_r.

AMS ^{14}C dating was performed on two intact bivalve shells from MB1L (260-265 cm, 439-444 cm). Conventional ^{14}C ages were calibrated using MARINE13. The calibration protocol corrects for a 400 yr global marine reservoir effect and a regional reservoir effect (ΔR) (Reimer et al., 2013). Moreton Bay is shown to have a depletion of the marine reservoir effect ($\Delta R = -216 \pm 94$ yrs.) compared to the modelled global ocean due to the presence of terrestrial carbon (Ulm et al., 2009).

More recent burial ages were determined using radionuclide dating. ^{137}Cs measurements were used to define the pre/post 1959 boundary (Hughes et al., 2009). Additional measurements including, ^{210}Pb and trace elemental (Pb-total) and loss on ignition (LOI) trends were used to determine the stratigraphic relationship of cores MB1S and MB1L. Conventional ^{210}Pb dating techniques (constant rate of supply (CRS) / constant initial concentration (CIC)) were not applicable this setting due to the inability to account for ^{210}Pb supplied through both direct fallout and via sediments loads of rivers entering the bay.

3.4 Geochemistry and grain size analysis

For geochemistry, 2 cm intervals were sampled contiguously for MB1S, while from MB1L 5 cm intervals were sampled from 0 to 100 cm and 10 cm intervals were sampled from 100 to 444 cm.

Major elements were determined by inductively coupled plasma optical emission spectrometry (ICP-OES) on samples digested by lithium metaborate fusion on a kantaxa automatic fluxer. 100 mg of sample was added to 1.0 g of lithium metaborate in a clean platinum crucible and placed in a furnace. Following heating in the furnace, the sample and molten flux was transferred to a PFA beaker containing 100 ml of a 4.0 % HNO_3 / 2.0 % HCl solution. The solution was diluted by 1:9 with reagent water into a 10 mL PPE tube. Aluminium and calcium were measured simultaneously on Agilent technologies 700 Series ICP-OES (uncertainty: Al-10 %, Ca-10 %, Practical quantification limit (PQL): Al-0.01 %, Ca-0.05 %), with PQL calculated based on the results of ten digest blanks; PQL = 3 (mean + 3 standard deviation). Calculated aluminium and calcium concentrations of dry sediment were then converted to weight percent oxides (Al_2O_3, CaO) based on loss on ignition (LOI) for individual samples. For grain size, 5 cm intervals were sampled contiguously in both MB1S and MB1L. Grain size distribution was measured using laser diffraction (Mastersizer 2000 - Malvern Instruments Ltd, UK). Grain size statistics including; sorting, skewness and kurtosis were calculated using the software GRADISTAT version 8.0 (Blott and Pye, 2001), and classified using the method of Folk and Ward (1957).

3.5 $\delta^{13}C$ and C/N ratios

For $\delta^{13}C$ 2 cm intervals were sampled contiguously for MB1S, while for MB1L 5 cm intervals were sampled. The $\delta^{13}C$ and C/N ratios of organic matter preserved in core samples were determined by IRMS as described in section 3.1.

3.6 Diatoms

For diatoms, 1 cm intervals were sampled every other centimetre for MB1S (i.e. 0-1, 2-3, etc.). For MB1L, 1 cm intervals were sampled at 4 cm intervals from 0 to 134 cm depth and at 6 cm intervals from 134 to 254 cm depth. Treatment of diatom samples followed Battarbee *et al.* (2001) and used standard hydrochloric acid and hydrogen peroxide digestion techniques. The digested material was deposited on coverslips, dried at room temperature, and mounted on slides using a Naphrax mounting

agent. Slides were traversed using a Nikon Eclipse E600 light microscope, under differential interference contrast (DIC) at 1500 x magnification, along vertical transects of known co-ordinates as recommended by Battarbee *et al.*, (2001) to achieve counts of >200 valves per sample. References to Desikachary (1988a, b, 1989), Krammer and Lange-Bertalot (1986, 1988, 1991a, b) and Witkowski *et al.* (2001) were made for the identification of all taxa. Diatom species/groups were classified by their environment as continental (C) (live in fresh water), estuarine/brackish (E/B) (euryhaline) or marine (M). Estuarine/brackish and marine diatoms are assumed to be autochthonous in the bay and were also classified as predominantly benthic or planktonic based on available literature (e.g. Desikachary *et al.*, (1988a)) Continental diatoms were also separated into their major growth forms including; planktonic, benthic and aerophilous.

3.7 Record integration and indexation

A simple indexation method based on the number of proxy records that indicated either increased or decreased discharge was employed to generate the final record of freshwater discharge. Values of each proxy for individual years were determined using linear interpolation based on the age-depth relationship. This allowed direct comparisons to be made between individual years, and the development of an integrated climate record. For individual proxies the inferred degree of freshwater discharge was determined from the degree of deviation from the average of the data set in the direction that indicated increased freshwater discharge (e.g. Al_2O_3/CaO = > 0). The proxies included in the integration were; Al_2O_3/CaO, < 10 μm, $\delta^{13}C$, C/N and the diatom *Paralia fenestrate (P. fenestrata)*. *P. fenestrata,* a marine species, which was the most common diatom present in the record representing between ~60 ~85 % of the assemblage. Reduced abundances of this dominant diatom in the final record typically coincided with an increase in abundance of the typically estuarine diatom *Cyclotella litoralis.* Therefore, the relative abundance of *P. fenestrata* was likely to provide the most relevant estimate of altered average water salinity at this site through time. Values of 2 and 0 were assigned to individual years for each proxy, indicating high and low freshwater influence. Because the diatom record is not complete, an intermediate value (1) was assigned to the period with no data for *P. fenestrata* abundance.

Summed scores for individual years of < 5 indicated a probable decrease in freshwater discharge and a drier climate overall was inferred, while scores > 5 indicated a probable increase in freshwater discharge and a wetter climate was inferred.

4. Results

4.1 Bay-wide survey

The $\delta^{13}C$ values ranged from -25.1 ‰ to -9.0 ‰ with an average of -20.9 ‰. The spatial variability of $\delta^{13}C$ is typical of an estuarine mixing zone, ranging from relatively low values of - 25 ‰ to -22.0 ‰ within the estuarine reach of the Brisbane River, and higher values of -21 to -18.0 % within western Moreton Bay and more oceanic sites. Three sites (BS 1, 2, 5) located within the sandy calcareous sediments of Waterloo Bay (Fig. 1), close to the Brisbane River mouth contrasted with this general trend with much lower values than the average for the data set (-14.9 ‰, -12.9 ‰, -9.0 ‰). TOC in sediments ranged from 0.19 - 2.38 % with an average of 0.92 %. TN ranged from 0.01 – 1.05 % with an average of 0.11 %. C/N ratios range from 7 - 29, averaging 12.2. Two outliers of 0.5 and 0.67 were observed for BS 3 and BS 6, respectively.

Bivariate correlations between $\delta^{13}C$ (‰), TOC (%), TN (%) and C/N ratios of bottom sediments and 5 year average monthly water quality variables (Chlorophyll a (Chl a), Salinity, Secchi depth, TN, TP, DO, pH, Temperature and Turbidity) for equivalent sites are presented in Table 1. This analysis excludes the outliers (BS 1, 2, 3, 5, 6). The $\delta^{13}C$ is significantly ($p = < 0.005$) positively correlated with salinity, secchi depth and pH ($r = +0.72, +0.75, +0.71$), and strongly negatively correlated with turbidity ($r = -0.67$). Non-linear regression also shows the strength of the relationship between salinity, secchi depth and the $\delta^{13}C$ (‰) values of bottom sediments (with $r^2 = 0.64$, and 0.65 respectively) ($p = < 0.005$) (Fig. 2). C/N ratios of organic matter in bottom sediments are also moderately negatively correlated with salinity, secchi depth and pH ($r = -0.35, -0.39, -0.39$) ($p = < 0.005$), while positively correlated with turbidity ($r = 0.40$ $p = < 0.005$). Moderately inverse relationships are seen between salinity, secchi depth and C/N ratios when regressed using non-linear methods ($r^2 = 0.24, 0.20$) (Fig. 2). Ordinary

kriging in Arc GIS was used to interpolate values to un-sampled sites to generate contour maps, with outliers excluded (Fig. 3).

4.2 Geochronology

The OSL and AMS ^{14}C ages show good agreement (Table 2). The basal ages of MB1L are within one sigma error (OSL: 1445 ± 145, AMS 14C: 1430 ± 110 years ago). Figure 4 summarizes the dating methods and results. Sediment deposited after 1959 was identified by the detection of ^{137}Cs, while a distinctive viscous layer at the sediment surface was determined to be sediment deposited during the 2011 flood. Intervening ages of the short core (MB1S) were determined using linear interpolation, in the absence of a more detailed (i.e. ^{210}Pb based) chronology for young sediments. For deeper sediments, an age model was defined using linear regression of both the OSL and ^{14}C ages, which was suggestive of long-term linear sedimentation at this site (Fig. 4b). The linear relationship between age and depth in core MB1L also suggests that there are no major hiatuses in the record. However, it is possible that a hiatus exists between the top of the long (MB1L) and base of the short core (MB1S), and the basal sample of MB1S may not represent the maximum depth of detectable ^{137}Cs (Fig 4a). The shallowest detection of ^{137}Cs at neighbouring core site (MB2) occurred at 59 cm (Coates-Marnane et al., 2016). Although, the base of MB1S may not represent the year 1959, based on core LOI and trace elements (Pb) profiles of the two cores it is unlikely that a considerable gap (>10 years) has been missed in the record.

4.3 Geochemistry and grain size analysis

The entirety of the sediment profile consisted of organic rich medium silts, with accessory fine sand (63–125 μm), and occasional shell fragments (D50 ~ 8.2 μm). Grain size analysis identified little variation down core with all samples classified as poorly sorted, coarsely skewed mesokurtic silt. Grain size analysis and geochemistry was used to investigate the contribution of terrestrial (aluminosilicate) and marine (calcium carbonates) components of the sediments to different grain size classes. Strong

positive relationships are shown for Al_2O_3/CaO and sediments sized between 4 – 16 µm and < 10 µm, while strong inverse relationships are shown for Al_2O_3/CaO and sediments sized between 16 – 62.5 µm (Fig. 5). This implies that there is an increasing contribution of CaO in the silt fraction, and an increasing contribution of Al_2O_3 in clay sediments. Calcifying foraminiferans were observed in relatively high numbers in sediments < 63 µm. The presence of both foraminiferans and other shell fragments is increasing the CaO contribution in equivalent sediments. The ratio Al_2O_3/CaO can therefore be used as an indicator of the relative contribution of terrestrial (aluminosilicate) vs marine (calcium carbonate) material to the sediment mixture deposited on the bay floor. Similarly, the proportion of <10 µm material in sediments can be used as an indicator of the relative proportion of terrestrial aluminosilicate clays in bottom sediments – and, by inference, an indicator of river discharge.

4.4 Core profile trends

The record including measurements of sediments sized < 10 µm, Al_2O_3/CaO ratio, $\delta^{13}C$ ‰ and C/N values, and the relative abundance of diatom species *Paralia fenestrata*, *Cyclotella litoralis*, and continental species extends from ~630 to 2011 CE (Figure 6). The scale of the ages of more recently deposited sediments, including those deposited after 1959 and as a result of the 2011, has been emphasized to highlight trends of this historical era. The diatom record does not extend prior to 1200 CE.

Sediments sized < 10 µm (%) ranged from 49.5 to 62.5 %, averaging 56.1 %. The Al_2O_3/CaO ratio ranged from 4.7 to 12.5 with an average of 6.8. The trend of the < 10 µm fraction of sediment exhibits a similar trend to the Al_2O_3/CaO ratio. Between 630 and 1200 CE both the < 10 µm (%) and the Al_2O_3/CaO ratio is generally below the average of the record. Between 1200 to ~1900 CE < 10 µm (%) and the Al_2O_3/CaO ratio are generally above average, with high values occurring between 1500 and 1900 CE. The period of European settlement beginning ~1840, and particularly the period after 1959, is characterized by dramatic shifts in sediment geochemistry and particle size. The < 10 µm

fraction and the Al_2O_3/CaO ratio decrease significantly after 1959 followed by a sharp increase in the 2011 flood layer.

The $\delta^{13}C$ values (‰) of sediments at the core site ranged from -21.3 ‰ to -19.4 ‰, with an average of - 20.1 ‰. C/N ratios ranged from 9.4 to 13.4 with an average of 10.6. These values are broadly consistent with the $\delta^{13}C$ ‰ and C/N of bottom sediments sampled in the same region in November 2013 (Fig. 3). Down-core variations in $\delta^{13}C$ and C/N ratios are subtle, though there are a few prominent features. The $\delta^{13}C$ ratios of organic matter are generally relatively high between 630 and 1200 CE (-20.1 ‰ to -19.3 ‰, average -19.7 ‰), peaking between ~1050 to ~1100 CE at ~19.3 ‰. The $\delta^{13}C$ ratios decrease slightly between 1300 to 1500 CE, averaging ~20.0 ‰ between ~1500 to 1900 CE. Values decrease significantly from ~1900 to the present, with a shift of – 1.1 ‰. Flood-derived sediment has the lowest $\delta^{13}C$ values of 20.8 – 21.1 ‰. C/N ratios are significantly higher for flood sediments than the remainder of the record (11.1 – 13.4 ‰). However, there is no correlation between the C/N and $\delta^{13}C$ ratios for the sediment profile ($r^2 = 0.04$).

The majority of diatoms observed in the sediment record were marine, and were dominated by the marine diatom *Paralia fenestrata*. Continental and estuarine/brackish diatoms were also a major component of the assemblage. The relative abundance of marine diatom *P. fenestrata* ranged from 1.5 – 94 %. The highest abundances occurred early in the record between 1200 and 1500 CE (53 – 94 %). Between 1500 and 1700 CE the relative abundance of *P. fenestrata* falls below 40 % averaging 47 %. Their abundance remains relatively constant (~50 %), from ~1800 to 1990 CE. A rapid decrease in abundance is seen for sediment deposited after 1990 CE, particularly in 2011. *Cyclotella litoralis* is an estuarine diatom species that typically occurs within the littoral zone in brackish waters. The decrease in abundance of the dominantly marine diatom *P. fenestrata* between 1500 and 1700 CE is paired with a marked increase in *C. litoralis*, increasing from < 20 % to 30 – 40 % for this period. The relative abundance of this diatom for the remainder of the record is relatively constant, typically < 20 %. Continental diatoms occur at greatest abundances between 1550 CE and 1750 and between 1850 and 2011. High abundances of continental diatoms as seen in sediments derived from the 2011 flood (25 %)

are also found at two key intervals corresponding to the years 1646 and 1683 CE (23 % and 16 % respectively). Key continental diatoms observed in the record included aerophilious *Aulacoseira* species and planktonic *Luticola* species. In 2011 the total abundance of both planktonic and benthic continental diatoms in sediments is comparable to the peaks observed in the 1600s (Fig. 7). However, the relative abundance of aerophilous diatoms, those typically originating from damp soils (i.e. river banks/ wetlands), was far greater in 2011 (1.8 to 6.4 %) than in the 1600s (0.5 to 1.0 %).

5. Discussion

5.1 Biogeochemical patterns in Moreton Bay

The spatial trends of $\delta^{13}C$ and C/N ratios in bed sediments in Moreton Bay reflect the mixing of terrestrial organic matter derived from C3 and C4 plants, with marine organic matter, principally from algae, cyanobacteria, and macrophytes. The mixing of these distinct sources produces a gradient, from more terrestrial influenced reaches in the Brisbane River estuary to more oceanic influenced sites within central Moreton Bay. This is consistent with patterns observed in similar settings in Australia and elsewhere (Zong et al., 2006). The link between this biogeochemical gradient and the physical mixing of fresh, estuarine and salt water is depicted by the relationship between $\delta^{13}C$ values and salinity and secchi depth (Figs 2, 3). The turbid and brackish waters of the upper Brisbane River estuary are characterized by relatively low $\delta^{13}C$ and high C/N values. Further downstream, $\delta^{13}C$ values increase owing to the greater relative contribution from marine aquatic plants and algae. Sediment $\delta^{13}C$ and C/N ratios reflect the mixing gradient between these two end members transitioning from freshwater terrestrial environments to saline, marine environments in Moreton Bay.

5.2 Contextualizing the late Holocene record using 2011 flood-derived sediments

The record developed at site MB1 encompasses the last ~1500 yr. As a result of the 2011 flood, 5-10 million tonnes of sediment was deposited and western Moreton Bay became fresh-brackish (<10 ppt salinity) for several days (EHMP, 2011; Stevens et al., 2014; Coates-Marnane et al., 2016). This

recent event allows for the characterization of the sedimentary signature of floods within the Moreton Bay record. Flood sediments from 2011 are rich in aluminosilicate clays, indicated by the high relative proportion of sediment < 10 μm, and increase in the Al_2O_3-CaO ratio (Fig. 6). Similarly, a relative decrease in $\delta^{13}C$ and increase in the C/N ratio of sediment indicates the deposition of terrestrial organic matter (Fig. 6). In addition, the relative abundance of continental diatoms is higher in flood sediments compared to previously deposited sediments (Fig 6). It is therefore reasonable to use these relative changes in sediment composition to reconstruct the past variability of freshwater discharge into the bay over the last 1500 years, with the assumption that similar relative changes in the composition of sediments should have occurred in response to periods of high flow. However, historical land-use changes have likely altered the biogeochemical characteristics of suspended sediments delivered to the bay. Similarly, the rate of fine sediment supply to the bay as a whole has increased since European settlement (Coates-Marnane et al., 2016). Given these changes, the signal of the 2011 flood in the bay is potentially unprecedented in terms of the depth of accretion of fine sediments in the central bay (0-10 cm). Despite the increase in rate of fine sediment accretion in Moreton Bay, based on grain size analysis no increase in the proportion of silt to sands is observed at this site in response to an increase in sedimentation. Considering this, we assume the proxies used here at this specific site have maintained a consistent response to variable river discharge through time. However, it is likely that the scale of the shifts in the proxies in response to modern floods has altered since anthropogenic modification of the catchment.

5.3 Long-term trends in river discharge

5.3.1 630 – 1300 CE

The integrated proxy record indicates a reduced river discharge between 630 and 1200 CE. The most probable explanation of this is below average rainfall in the catchment and a reduction in average freshwater discharge and frequency of flooding events, peaking in severity between 1050 to 1200 CE (Fig. 8). The occurrence of anomalously low rainfall and aridity across this period has been identified in a range of environments on the Australian mainland. Using diatom-inferred records of lake salinity

from the western plains of Victoria (Lake Elingamite and Surprise) Barr *et al.,* (2014) also identified a multi-decadal drought between 650 and 850 CE, and a period of high climate variability between 850 and 1400 CE. After 1400 CE the climate became wetter with a significant reduction in inter-decadal variability (Fig. 8). In addition, a recent ice core record from Law Dome Ice Sheet in Antarctica has been used to develop a high-resolution long-term (1000 years) drought record for subtropical eastern Australia (Vance et al., 2015). Two dry epochs were identified between 1000-1260 CE and 1920-2009 CE (Fig. 8). Finally, a recent reconstruction of flood activity over the last two millennia from Fortescue Marsh in the arid subtropics of northwest Australia revealed the period between 700 – 1600 CE was characterized by floods of reduced magnitude compared to those after 1600 CE (Rouillard et al., 2016).

5.3.2 Connections between regional drying and global climate

The inferred broad dry phase in many regions of Australia at the turn of the last millennia coincides with an increase in El Niño frequency based on a record from the Eastern Pacific. Using sediment grain size analysis of a sediment core from El Junco Lagoon in the Galapagos, Conroy *et al.,* (2008) inferred an increase in the frequency of El Niño events between ~600 to ~1300 CE. After 1,300 CE, El Niño events decreased in frequency and showed less variability (Fig. 8). Similarly, Moy et al., (2002) found a peak in the frequency of warm phase (El Niño) ENSO events at ~800 CE, with a subsequent decline toward the present. The overall drier, more variable climate between ~630 and ~1300 CE also occurs during the medieval climate anomaly (MCA). In the Northern Hemisphere, the MCA occurred between 950 and 1200 CE (Mann et al., 2009), however no global coherent warm phase during medieval times was identified (Neukom et al., 2014). Despite this, there is some evidence for the occurrence of a significant climate anomaly in the Southern Hemisphere similar to that described as the MCA, characterized by anomalously warm conditions (Cook et al., 2002; Kemp et al., 2012; Neukom et al., 2014). Using multiple temperature reconstructions from Australasia spanning 1000 – 2001 CE Gergis *et al.,* (2016) also identified a peak in preindustrial warmth between 1150 and 1350 CE. Drought frequency and severity in eastern Australia at this time may have been exacerbated by

increased evaporation in response to anomalously warm conditions in combination with increased El Niño frequency and intensity.

5.3.3 1300 – 1700 CE

The record suggests an average increase in discharge to the bay between 1300 and 1900 compared to prior to 1200 CE. The peak in this wet period occurs between 1500 and 1700 CE as evidenced by the high abundance of continental diatoms at this time (Fig. 7). This is followed by a return to relatively dry conditions and reduced river discharge between 1700 and 1850 and subsequently by an onset of increased river discharge after 1850 continuing at least until 1900. Climate reconstructions in the austral Pacific also indicate an especially wet epoch extending from ~1400 to ~1900 CE (Yan et al., 2011; Vance et al., 2015). Croke *et al.*, (2016) developed a millennial scale record of flooding in the Lockyer Valley catchment of the upper Brisbane River, based on OSL ages of flood deposits. Their evidence indicates that floods comparable to the January 2011 event have occurred several times over the last 2,000 years, with flood activity peaking around 1730 CE. This finding is in broad agreement with the Moreton Bay record suggesting peak flooding activity in the late 1600s.

5.3.4 Connections between regional rainfall increases and global climate

The decrease in frequency of strong El Niño phases of ENSO throughout the last millennia as identified in the Galapagos (Conroy et al., 2008) may partially explain the transition from a drier climate at the turn on the last millennia to a wetter climate in the latter half of the last millennia in the Moreton Bay catchment. In addition, the transition from 'dry' conditions at the turn of the last millennia to a 'wetter' climate by 1300 to 1400 CE is also broadly synchronous with the transition from the MCA to the Little Ice Age (LIA). The LIA, characterized by hemispheric-scale cooling, occurred between 1400 and 1850 CE in the North Atlantic region (Mann et al., 2009). Unlike the MCA, annually resolved temperature reconstructions of the Southern and Northern Hemispheres, suggests strong inter-

hemispheric coupling during the peak of the LIA (1600 – 1700 CE) (Neukom et al., 2014). A recent compilation of temperature records from the Australasian region also identified a shift toward cooler climates after 1500 CE (PAGES 2k Consortium, 2013). Similarly, Gergis *et al.,* (2016) identified a transition to cooler conditions in Australasia after ~1350 CE.

This mid-millennia cooling trend (LIA) was also characterized by a gradual southward displacement in the position of the inter-tropical convergence zone (ITCZ) (Haug et al., 2001; Sachs et al., 2009). The displacement of the ITCZ over the last millennia has strongly influenced rainfall variability in the tropics over the past millennia (Lechleitner et al., 2017). Lechleitner *et al.,* (2017) found that the most prominent period of southward (negative) deflection of the ITCZ occurred between 1320 and 1820 CE and corresponded to increased rainfall in the Southern Hemisphere tropics. A more pronounced influence of the ITCZ in the Southern Hemisphere during this period may have translated into an increase in rainfall in the Australian subtropics, through a greater southward influence of rain producing features associated with the Australian monsoon and tropical cyclones. Elevated tropical cyclone activity in north eastern Australia (Chillagoe) is also indicated from ~1500 CE to ~1800 CE based on speleothems (Haig et al., 2014). Rouillard *et al.,* (2016) also provides evidence for the initiation of a period of intense flooding coincident with the LIA, highlighting the southward deflection of the ITCZ as a potential mechanism for increased regional precipitation. Together, this is suggestive of geographically broad, synchronous, hrydoclimatic change in northern Australia in response to global cooling.

The ITCZ displacement is also known to strongly influence the relative activity of modern ENSO, which may have influenced rainfall variability in east coast Australia (Rustic et al., 2015). The interactions of ENSO, hemispheric cooling and the meridional displacement of the ITCZ over the past millennium remain challenging to investigate due to the scarcity of highly resolved records. The transition to a wetter La Niña -like climate from 1300 to 1680 CE observed in this record was likely caused by a combination of the dynamic interactions of several climate drivers. Other potential influences on subtropical and tropical rainfall which warrant further investigation into their variability

over the last several millennia include the Southern Annular Mode (SAM) and the Madden Julian Oscillation (MJO) (Hall et al., 2001; Goodwin et al., 2014).

The increase in river discharge over the last millennia is briefly interrupted by a period of reduced discharge between ~1700 and 1850 CE. A reconstruction of river discharge into the Great Barrier Reef (GBR) lagoon in 1648 – 2011 CE based on coral luminescence also highlights a period of decreased freshwater input between 1700 and 1850 CE (Lough et al., 2015). After the 1850s, freshwater flow into the GBR from its largest river, the Burdekin, increases. This coincides with a shift to a more La Niña like average climate state and an increase in ENSO variance. Rustic *et al.*, (2015) also identified a mid-millennium shift (MMS) in ocean-atmosphere circulation at ~1500 to ~1650 CE, which is suggested to correspond to an increase in general ENSO activity between ~1600 and ~1800 CE.

5.3.5 1900 to the Present

Deforestation of the catchment was initiated by the expansion of agriculture in the region in the early 20th century. Currently, < 25 % of the catchment's original vegetation remains (Capelin et al., 1998). This change in land cover, and expansion of grazing and cropping, has significantly transformed the hydrology and geomorphology of the catchment (Kemp et al., 2015; 2018). Inferences drawn from the relative changes of various proxies across this period are confounded this transformation. It remains challenging to decouple the effect of an increase in river influence as a result of either; 1) a climatic shift or 2) an increase in run-off efficiency and erosion associated with anthropogenic land use changes. In addition, the use of $\delta^{13}C$ values of sediments to infer the relative input of terrestrial carbon becomes problematic after 1900 due to the Suess effect (Keeling, 1979). The Suess effect describes the shifting ratio of atmospheric concentrations of heavy isotopes of carbon (^{14}C, ^{13}C) as a result of an increased supply of ^{13}C and ^{14}C depleted carbon sources from the anthropogenic burning of fossil fuels. As a consequence, most of the observed depleted $\delta^{13}C$ record after 1900 CE could arise from shifts in atmospheric $\delta^{13}C$.

Historical flood records provide evidence that the late 1800s period were characterized by a greater frequency of major floods compared to the early to mid-20th century (Kemp et al., 2015). Considering this, the resumption of above average river discharges for the region that occurred after 1850 as identified by this record and others has likely extended to the present day (Kemp et al., 2015; Lough et al., 2015). It is likely that natural increases in sediment yield of the catchment due to increased precipitation and run-off were also paired with increases related to land-use changes following European settlement (Coates-Marnane et al., 2016).

Three distinct peaks in total continental diatoms abundances occur in the record, corresponding to the 2011 flood and the years 1646 and 1683 CE. The major difference in these three peaks is ratio of aerophilous diatoms in the assemblages. A far greater contribution of the aerophilous growth forms is seen for the 2011 peak. Aerophilous diatoms often inhabit damp soils (Johansen, 1999). This suggests the floods earlier in the record although were likely to be of a similar magnitude to the 2011 flood, they were far less erosive. An increase in the quantity of eroded soils mobilized during high magnitude floods as a result of extensive land-use changes over the last 150 to 200 years is the most probable explanation for this distinction (Olley et al., 2013; Thompson et al., 2013; Kemp et al., 2015; 2018). Indeed, since European settlement in the region fine sediment accretion in the bay has increased by 3 to 9 fold (Coates-Marnane et al., 2016).

5.4 Record limitations

The long-term age depth relationship based on OSL and ^{14}C is suggestive of linear sedimentation over the long term. However, sedimentation at this site over the short term is clearly sporadic evidenced by rapid sedimentation following the recent 2011 flood. The long term linear age model may over or underestimate the depth of sediment deposited at certain intervals between each dated sediment horizon – increasing the uncertainty of the exact timing of shifts in the record. In addition, the relatively coarse long-term sampling resolution (i.e. 15 yr.) may be masking trends at the finer temporal scale. This record could be improved through additional OSL and ^{14}C dating of key

events or transitions identified by the proxies, especially the peaks of continental diatoms at ~1646 and ~1683 CE, with the aim of determining the precise age of past flood events.

5.5 Implications for water resource management in south-east Queensland

Climate records for the east coast of Australia over the last millennia suggest that the instrumental record does not cover the full range of climatic extremes experienced within the last 1500 years (Barr et al., 2014; Vance et al., 2015; Gergis et al., 2016). This conclusion is also supported by the current study. Water resource use in eastern Australia, for the purposes of agriculture, industry and urbanisation has grown rapidly within a relatively short time period (< 200 yrs.). As a result both public infrastructure and governing policies have been inherently tailored to suit a narrow range of natural climate variability in the context of the last 1500 years. Widespread flooding has caused significant damage to infrastructure in strong La Niña years such as 2011. Though similar magnitude floods have occurred in the recent past (< 500 yrs) evidence indicates that the highly erosive nature of the 2011 flood is potentially unprecedented in the last 1000 years, with complementary lines of evidence suggesting ongoing land cover/use changes in the catchment may be driving a trend toward more abrupt and erosive floods (Kemp et al., 2015). During flooding events in the south-east Queensland region high suspended sediment loads of rivers supplying major water treatment facilities have presented significant challenges in guaranteeing the adequate supply of portable water in the short term (SEQ Water, 2013). Not only do high magnitude floods threaten infrastructure but also the regions ability to secure a stable portable water supply.

The millennium drought also highlighted major deficiencies in the ability of eastern Australia's water planning policies and infrastructure to mitigate against widespread water shortages (van Dijk et al., 2013). Prolonged dry periods of greater magnitude than the millennial drought are also a natural feature of the climate of the region over the last 1500 years (Vance et al., 2015). It is evident that increased drying at the turn of the last millennia was accompanied by anomalously warm conditions. However, the warmest 30 year period in the Australasian region over the last millennia occurred after

the 1950s in response to anthropogenic greenhouse gases (Gergis et al., 2016). This implies that future anthropogenic climatic change may be compounded by already high natural long term (centennial scale) climate variability in Australia (Gergis et al., 2016), especially within the Australian subtropics.

The policy responses of local governing organisations to the water resource challenges faced in south-east Queensland since the 1970s are detailed by Head, (2014). The implementation of policy, by way of investments in new infrastructure and water efficiency initiatives were typically made following water crisis including the floods of 1974 and 2011, and the millennium drought. These events prompted new policy innovations and challenged old paradigms, however, Head (2014) suggests that despite the debate these crisis did not consolidate institutional capacity to plan collaboratively for the future. McGowan, (2012) also highlights that following the 2011 flood the Queensland Floods Commission of Inquiry produced recommendations focused on regulation and modelling and largely disregarded discourse around community resilience, disaster prevention and mitigation. The governance response to water resource challenges faced in the region in this instance could be considered as reactive - responding to immediate short term risks. A proactive approach that builds real resilience within catchments to both droughts and floods is now required to meet future water resource challenges. This approach requires a broad awareness of the inherent high variability of climate of the region, characterized by periods of intense flooding and severe droughts. The incorporation of this longer term perspective of regional climate and water availability into water governance will ultimately allow for more prudent and adaptable policy and planning.

6. Conclusions

This multi-proxy reconstruction of river discharge in central Moreton Bay over the last 1500 years identifies a prominent shift towards a wetter climate and increase in river discharge after 1300 CE, continuing to the present. The initial shift toward a cool Southern Hemisphere climate after 1300 CE accompanied a decrease in El Niño events and a reduction in ENSO overall activity, which most likely translated to an increase in average rainfall in the Australian subtropics. This shift is briefly

interrupted by a minor decrease in river discharge and return to a drier climate between ~1700 CE and 1850 CE. A return to a more La Niña like climate state after 1850 resulted in increased average rainfall and river discharges in the region. Resolving relative trends in river discharge in relation to climate variability after the 1850s in the region is confounded by the geomorphic transformation of the catchment following the clearing of forests and the introduction of agriculture. However, additional regional records suggest similar magnitude floods to that experienced in January 2011 have occurred several times within the last 1000 years peaking in frequency between 1500 CE and 1700 CE. In addition, prolonged dry periods similar, or of higher magnitude to the millennium drought are significant features of the climate of the region over the last 1000 years.

The paucity of data of low amplitude climate variability for the Australian continent limits our capacity to manage water resources under a changing climate. This research has demonstrated that coastal deltaic and shelf sediments can offer novel insights into climate variability of the recent past. Deltaic settings that are likely to show the greatest potential for inferring past river discharge include those that are protected from high energy oceanic conditions and within tectonically stable coastal margins, such as Moreton Bay. The understanding of climate over the last 1000 years would benefit from a greater number of climate reconstructions from tropical and subtropical climate zones. This would greatly improve our mechanistic understanding of present climate variability and the likely effects of continued global warming on shifts in ocean-atmosphere systems and the resulting impact on regional climates and water resources.

Acknowledgments

This project was funded by the Australian Research Council (ARC linkage project LP120100093). The Chemistry Centre of The Department of Environment and Science (DES) provided in-kind funding for vibracoring and diatom analyses. We thank Rob DeHayr and staff within the Chemistry Centre for geochemical analysis, expert technical advice and facilities use. We thank Jacky Croke for valuable discussions during the early stages of the project. Staff of the Ecosystem Health Monitoring (J. Ferris,

J. Gruythuysen, J. Fels, M. Waller, and K. Reeves) assistance with field sampling. Water Quality data was provided by the Ecosystem Health Monitoring Program, Healthy Waterways Ltd. Rad Bak and Renee Diocares performed the stable isotope analysis at Griffith Universities stable isotope facility.

References

Barr, C., Tibby, J., Gell, P.G., Tyler, J.J., Zawadzki, A., Jacobsen, G.E., 2014. Climate variability in south-eastern Australia over the last 1500 years inferred from the high-resolution diatom records of two crater lakes. Quat. Sci. Rev. 95, 115-131.

Battarbee R.W., Jones V.J., Flower R.J., Cameron N.G., Bennion, H., Carvalho L. and Juggins, S. 2001. Diatoms. In: Stoermer, E.F., Birks, H.J.B., Last, W.M. (Eds), Tracking environmental change using lake sediments. Volume 3: terrestrial, algal and siliceous indicators. Kluwer Academic Publishers Dordrecht, The Netherlands, pp. 155-202.

Bird, M.I., Brunskill, G.J., Chivas, A.R., 1995. Carbon-isotope composition of sediments from the Gulf of Papua. Geo-Marine Letters 15, 153–159.

Blott, S. J. and Pye, K. 2001. GRADISTAT: A grain size distribution and statistics package for the analysis of unconsolidated sediments, Earth Surf. Proc. Land. 26, 1237–1248.

Cai, W., Borlace, S., Lengaigne, M., van Rensch, P., Collins, M., Vecchi, G., Timmermann, A., Santoso, A., McPhaden, M.J., Wu, L., England, M.H., Wang, G., Guilyardi, E., Jin, F-F. 2014. Increasing frequency of extreme El Niño events due to greenhouse warming. Nat. Clim. Change, 4, 111–116.

Cai, W., Wang, G., Santoso, A., McPhaden, J.J., Wu, L., Jin, F-F., Timmermann, A., Collins, M., Vecchi, G., Lengaigne, M., England, M.H., Dommenget, D., Takahasi, K., Guilyardi, E. 2015. Increased frequency of extreme La Niña events under greenhouse warming. Nat. Clim. Change 5, 132–137.

Cai, W., van Rensch, P., 2012. The 2011 south eastern Queensland extreme summer rainfall: A confirmation of a negative Pacific Decadal Oscillation phase?, Geophys. Res. Lett., 39, L08702, doi: 10.1029/2011GL050820.

Capelin, M., Koln, P., Hoffenberg, P., 1998. Land use, land cover and land degradation in the catchment of Moreton Bay. In: Tibbetts, I.R., Hall, N.J., Dennison, W.C. (Eds.), Moreton Bay and Catchment. School of Marine Science, University of Queensland, Brisbane, Australia, pp. 3-54.

Chiew, F.H.S., Piechota, T.C., Dracup, J.A., McMahon, T.A., 1998. El Niño /Southern Oscillation and Australian rainfall, streamflow and drought: Links and potential for forecasting. Journal of Hydrology 204, 138–149.

Clement, A.J.H., Fuller, I. C., Sloss, C.R. 2017. Facies architecture, morphostratigraphy, and sedimentary evolution of a rapidly-infilled Holocene incised-valley estuary: The lower Manawatu valley, North Island New Zealand. Marine Geology 390, 214-233.

Cloern, J.E., Canuel, E.A., Harris, D., 2002. Stable carbon and nitrogen isotope composition of aquatic and terrestrial plants of the San Francisco Bay estuarine system. Limnology and Oceanography 47, 713–729.

Coates-Marnane, J., Olley, J., Burton, J., Sharma, A., 2016. Catchment clearing accelerates the infilling of a shallow subtropical bay in east coast Australia. Estuarine, Coastal and Shelf Science 174, 27-40.

Conroy, J.L., Overpeck, J.T., Cole, J.E., Shanahan, T.M. & Steinitz-Kannan, M. 2008. Holocene changes in eastern tropical Pacific climate inferred from a Galápagos lake sediment record. Quaternary Science Reviews 27, 1166–1180.

Cook, E., Palmer, J., and D'Arrigo, R. 2002. Evidence for a "Medieval Warm Period" in a 1100- year tree-ring reconstruction of past austral summer temperatures in New Zealand. Geophysical Research Letters 29 (14), 1667.

Cook, E.R., Buckley, B.M., D'Arrigo, R.D., Peterson, M.J. 2000. Warm-season temperatures since 1600 BC reconstructed from Tasmanian tree rings and their relationship to large-scale sea surface temperature anomalies. Climate Dynamics 16, 79-91.

Croke, J.C., Fryirs, K.A., Thompson, C.J. 2013. Channel-floodplain connectivity during an extreme flood event: Implications for sediment erosion, deposition, and delivery. Earth Surface Processes and Landforms 38, 1444–1456.

Croke, J.C., Thompson, C.J., Denham, R., Haines, H.A., Sharma, A., Pietsch, T. 2016. Reconstructing a millennial-scale record of flooding in a single valley setting: the 2011 flood-affected Lockyer Valley, SEQ, Australia. Journal of Quaternary Science 31 (8), 936-952.

Day, R.W., Whitaker, W.G., Murray, C.G., Wilson, I.H., Grimes, K.G., 1983. Queensland geology, a companion volume to the 1:2500000 scale geological map (1975). Geological Survey of Queensland Publication, p. 383.

De Dekker, P., Barrows T. T., Rogers, J. 2014. Land-sea correlations in the Australian region: post-glacial onset of the monsoon in northwestern Western Australia. Quarternary Science Reviews 105, 181-194.

Dennison, W., Abal, E. G., 1999. Moreton Bay study: a scientific basis for the Healthy Waterways Campaign, Brisbane, Qld., South East Queensland Regional Water Quality Management Strategy, p. 245.

Department of Natural Resources and Mines (DNRM), Queensland Government 2016. Queensland spatial catalogue. http://qldspatial.information.qld.gov.au/catalogue/custom/index.page.

Desikachary, T.V. 1988a. Atlas of Diatoms. Fascicle 3-4. Diatoms from the Bay of Bengal/ Marine Diatoms from the Arabian Sea and Indian Ocean (1st Edition). Madras Science Foundation, J.J. Maps & Publications, Madras.

Desikachary, T.V. 1988b. Atlas of Diatoms. Fascicle 5. Marine Diatoms of the Indian Ocean region (1st Edition). Madras Science Foundation, J.J. Maps & Publications, Madras.

Desikachary, T.V. 1989. Atlas of Diatoms. Fascicle 6. Marine Diatoms of the Indian Ocean region (1st Edition). Madras Science Foundation, J.J. Maps & Publications, Madras.

EHMP. 2011. Ecosystem Health Monitoring Programme 2010–2011 Annual Technical Report. Moreton Bay Waterways and Catchments Partnership, Brisbane.

Emery, K.O., Wigley, R.L., Bartlott, A.S., Rubin, M., Barghoorn, E.S. 1967. Freshwater peat on the continental shelf. Science 158, 130–137.

Evans, K. G., Stephens, A., W Shorten, G. G. 1992. Quaternary sequence stratigraphy of the Brisbane River Delta, Moreton Bay, Queensland, Australia. Marine Geology 107, 61-79.

Folk, R. L. and Ward, W. C. 1957. Brazos River bar [Texas]; a study in the significance of grain size parameters, J. Sediment. Res. 27, 3–26.

Fontugne, M.R. and Jouanneau, J.M. 1987. Modulation of the particulate organic carbon flux to the ocean by a macrotidal estuary: evidence from measurements of carbon isotopes in organic matter from the Gironde Estuary. Estuarine Coastal and Shelf Science 24, 377- 87.

Fry, B., Scalan, R.S., Parker, P.L. 1977. Stable carbon isotope evidence for two sources of organic matter in coastal sediments: seagrass and plankton. Geochim. Cosmochim. Acta 41, 1875–1877.

Galbraith, R. F., Roberts, R. G., Laslett, G. M., Yoshida, H. Olley, J. M., 1999. Optical dating of single and multiple grains of quartz from Jinmium rock shelter, northern Australia, Part 1, Experimental design and statistical models. Archaeometry 41, 339-364.

Gallant A.J.E., Phipps S.J., Karoly D.J., Mullan A.B., Lorrey A.M. 2013. Nonstationary Australasian teleconnections and implications for paleoclimate reconstructions. Journal of Climate, 26, 8827-8849.

Gergis, J., Neukom, R., Gallant, A.J.E., Karoly, D. 2016 Australasian temperature reconstructions spanning the last millennium. Journal of Climate 29, 5365-5392.

Grinham, A., Gale, D., Udy. J. 2011. Impact of sediment type, light and nutrient availability on benthic diatom communities of a large estuarine bay: Moreton Bay, Australia. Journal of Paleolimnology 46, 511-523.

Grove, J.R., Croke, J., Thompson, C., 2013. Quantifying different riverbank erosion processes during an extreme flood event. Earth Surf. Process. Landforms 38 (12), 1393-1406.

Goodwin, I., Browning, S., Lorrey, M.A., Mayewski, P.A., Phillips, S.J., Bertler, N.A.N., Edwards, R.P., Cohen, T.J., vas Ommen, T., Curran, M.., Barr, B., Curt Stager, J. 2014. A reconstruction of extratropical Indo–Pacific sea-level pressure patterns during the Medieval Climate Anomaly. Clim.Dynam. http://dx.doi.org/doi:10.1007/s00382-013-1899-1.

Haig, J., Nott, J., Reichart, G., 2014. Australian tropical cyclone activity lower than at any time over the past 550-1,500 years. Nature 505 (7485), 667-672.

Haines, H., Olley, J. 2017. The implications of regional variations in rainfall for reconstructing rainfall patterns using tree rings. Hydrological Processes 31(16), 2951–2960.

Hall, J., Matthews, A., Karoly, D. 2001. The modulation of tropical cyclone activity in the Australian region by the Madden–Julian Oscillation. Mon Weather Rev 129, 2970–2982.

Hanna, A.J.M., Shanahan, T.M., Mead, A. A., Bianchi, T. S., Schreiner, K M. 2018. A multi-proxy investigation of late-Holocene temperature change and climate-driven fluctuations in sediment sourcing: Simpson Lagoon, Alaska. The Holocene, doi.org/10.1177/0959683617752845

Haug, G., Hughen, K.A., Sigman, D.M., Peterson, L.C., Rohl, U. 2001. Southward migration of the inter-tropical convergence zonethrough the Holocene. Science 293, 1304–1308.

Head, B. W. 2014. Managing urban water crises: adaptive policy responses to drought and flood in Southeast Queensland, Australia. Ecology and Society 19 (2): 33.

Hughes, A.O., Olley, J. M., Croke, J. C., McKergow, L.A.M., 2009, Sediment source changes over the last 250 years in a dry-tropical catchment, central Queensland, Australia. Geomorphology 104 (3-4) 262-275.

Johansen, J.R. 1999. Diatoms of aerial habitats. In: Stoermer, E.F., Smol, J.P. (Eds). The Diatoms: Applications for the Environmental and Earth Sciences. Cambridge University Press: Cambridge. pp. 264-273.

Keeling, C. D. 1979 The Suess effect: 13Carbon-14Carbon interrelations. Eviron. Int. 2, 229-300.

Kiem, A. S., Verdon- Kidd, D. C. 2013. The importance of understanding drivers of hydroclimatic variability for robust flood risk planning in thecoastal zone. Australian Journal of Water Resources 17, 126–134.

Kemp, J., Radke, L.C., Olley, J., Juggins, S., De Deckker, P. 2012. Holocene lake salinity changes in the Wimmera, southeastern Australia, with evidence for millennial-scale climate variability. Quaternary Research 77, 65-76.

Kemp, J., Olley, J.M., Ellison, T., McMahon, J., 2015. River response to European settlement in the sub-tropical Brisbane River, Australia. Anthropocene 11, 48-60.

Kemp J, Olley J, Capon S. 2018. An environmental history of Moreton Bay hinterlands. In: Tibbetts I.R., Rothlisberg, P.C., Neil, D.T., Homburg, T.A., Brewer, D.T., Arthington, A.H. (Eds). Moreton Bay (Quandamooka) & Catchment. MBQC2016, Brisbane. , Available at https://:www.mbqc2016.org/book.

Krammer, K., Lange-Bertalot, H. 1986. Bacillariophyceae, 1 Teil: Naviculaceae. in: Ettl H, Gärtner G, Gerloff J, Heynig H and Mollenhauer D (Eds) Süβwasserflora von Mitteleuropa, Band 2/1, Stuttgart/Jena: Gustav Fischer Verlag, 876 pp.

Krammer, K., Lange-Bertalot, H. 1988. Bacillariophyceae, 2 Teil: Bacillariaceae, Epthimiaceae, Surirellaceae. In: Ettl, H., Gärtner, G., Gerloff, J., Heynig, H., Mollenhauer, D. (Eds) Süβwasserflora von Mitteleuropa, Band 2/2, Stuttgart/Jena: Gustav Fischer Verlag, 596 pp.

Krammer, K., Lange-Bertalot, H. 1991a. Bacillariophyceae, 3 Teil: Centrales, Fragilariaceae, Eunotiaceae. In: Ettl, H., Gärtner, G., Gerloff, J., Heynig, H., Mollenhauer, D. (Eds). Süβwasserflora von Mitteleuropa, Band 2/3, Stuttgart/New York: Gustav Fischer Verlag, 576 pp.

Krammer, K., Lange-Bertalot, H. 1991b. Bacillariophyceae, 4 Teil: Achnanthaceae, Kritische Ergänzungen zo Navicula (Lineolatae) und Gomphonema Gesamtliteraturverzeichnis Teil 1-4. In: Ettl, H., Gärtner, G., Gerloff, J., Heynig, H., Mollenhauer, D. (Eds). Süβwasserflora von Mitteleuropa, Band 2/4, Stuttgart/New York: Gustav Fischer Verlag, Stuttgart, 437 pp.

Lam, D., Croke, J., Thompson, C., Sharma, A. 2017. Beyond the gorge: Palaeoflood reconstruction from slackwater deposits in a range of physiographic settings in subtropical Australia. Geomorphology 292, 164-177.

Lamb, A.L., Wilson, G.P., Leng, M.J., 2006. A review of coastal palaeoclimate and relative sea-level reconstructions using $\delta^{13}C$ and C/N ratios in organic material. Earth Science Reviews 75(1-4), 29–57.

Lechleitner, F. A., Breitenbach, S.F., Rehfeld, K., Ridley, H.E., Asmerom, Y., Prufer, K.M., Marwan, N., Goswami, B., Kennet, D.J., Aquino, V.V., Polyak, V., Haug, G.H., Eglinton, T.I., Baldini, J.U.L. 2017. Tropical rainfall over the last two millennia: evidence for a low-latitude hydrologic seesaw 7, 45809. DOI: 10.1038/srep45809.

Lewis, S.E., Sloss, C.R., Murray-Wallace, C.V., Woodroffe, C.D. Smithers, S.G., 2008. Post-glacial sea-level changes around the Australian margin: a review. Quaternary Science Reviews 74, 115-138.

Lockington, J.R., Albert, S., Fisher, P.L., Gibbes, B.R., Maxwell, P.S. Grinham, A.R., 2017. Dramatic increase in mud distribution across a large sub-tropical embayment, Moreton Bay, Australia. Marine Pollution Bulletin 116, 491-497.

Lough, J.M. Lewis, S.E. Cantin, N.E. 2015. Freshwater impacts in the central Great Barrier Reef: 1648- 2011. Coral Reefs 34, 739- 751.

Mann, M.E., Zhang, .Z, Rutherford, S., Bradley, R.S., Hughes, M.K., Shindell, D., Ammann, C., Faluvegi, G., Ni, F. 2009. Global signatures and dynamical origins of the Little Ice Age and Medieval Climate Anomaly. Science 326, 1256–1260.

McGowan, 2012. A Missed Opportunity to Promote Community Resilience? – The Queensland Floods Commission of Inquiry. Australian Journal of Public Administration 71 (3), 355-363.

McMahon, J. M., Olley, J. M., Brooks, A. P., Smart, J.C.R., Rose, C.W., Curwen, G., Spencer, J., Stewart-Koster, B. 2017. An investigation of controlling variables of riverbank erosion in sub-tropical Australia. Environmental Modelling & Software 97, 1-15.

Moy, C.M., Seltzer, G.O., Rodbell, D.T., Anderson, D.M., 2002. Variability of El Nino/Southern Oscillation activity at millennial timescales during the Holocene epoch. Nature 420, 162-165.

Neukom, R., Gergis, J., Karoly, D., Wanner, H., Curran, M., Elbert, J., González-Rouco, F., Linsley, B., Moy, A. D., Mundo, I. A., Raible, C. C., Steig, E. J., Van Ommen, T., Vance, T., Villalba, R., Zinke, J., Frank, D. 2014. Inter-hemispheric temperature variability over the past millennium, Nature Climate Change 4, 362–367.

Olley, J., Burton, J., Smolders, K., Pantus, F., Pietsch, T., 2013. The application of fallout radionuclides to determine the dominant erosion process in water supply catchments of subtropical south-east Queensland, Australia. Hydrol. Proc. 27, 885–895.

Olley, J.M., Pietsch, T., Roberts, R.G., 2004. Optical dating of Holocene sediments from avariety of geomorphic settings using single grains of quartz. Geomorphology 60, 337-358.

Owen, R.B., Neller, R.J., Shaw, R. Cheung, P.C.T. 1998. Late Quaternary environmental changes in Hong Kong. Palaeogeography, Palaeoclimatology, Palaeoecology 138, 151-73.

PAGES 2k Consortium. 2013. Continental-scale temperature variability during the past two millennia. Nature Geoscience 6, 339 -345.

Power, S., Callaghan, J., 2016. Variability in severe coastal flooding in south-eastern Australia since the mid-19th century, associated storms and death tolls. Journal of Applied Meterology and climatology 55 (1), 1139-1149.

Power, S.B., Delage, F.P.D., Chung, C.T.Y., Ye, H., Murphy, B.F. 2017. Humans have already increased the risk of major disruptions to Pacific rainfall. Nature Communications DOI:10.1038/ncomms14368

Power, S., Haylock, M., Colman, R., Wang, X., 2006. The predictability of interdecadal changes in ENSO activity and ENSO teleconnections. J. Clim. 19, 4755–4771.

Ramsay, H., Camargo, S., Kim, D. 2012. Cluster analysis of tropical cyclone tracks in the Southern Hemisphere. Clim. Dyn. 39, 897–917.

Reimer, P.J., Bard, E., Bayliss, A., et al., 2013. IntCal13 and MARINE13 radiocarbon age calibration curves 0–50000 years cal BP. Radiocarbon 55(4), 1869-1887.

Risbey, J.S., Pook, M.J., McIntosh, P.C., Wheeler, M.C., Hendon, H.H . 2009. On the Remote Drivers of Rainfall Variability in Australia. Monthly Weather Review 137, 3233–3253.

Rodriguez-Ramirez, A., Grove, C.A. Zinke, J., Pandolfi, J.M., Zhao, J-X. 2014. Coral Luminescence Identifies the Pacific Decadal Oscillation as a Primary Driver of River Runoff Variability Impacting the Southern Great Barrier Reef. PLoS ONE 9 (1), e84305. doi:10.1371/journal.pone.

Rouillard, A., Skrzypek, G., Turney, C., Dogramaci, S., Hua, Q., Zawadski, A., Reeves, J., Greenwood, P., O'Donnel, A.J., Grierson, P.F. 2016. Evidence for extreme floods in arid subtropical northwest Australia during the Little Ice Age chronozone (CE 1400-1850). Quarternary Science Reviews 144, 107-122.

Roy, P.S., Williams, R.J., Jones, A.R., Yassini, I., Gibbs, P.J., Coates, B., West, R.J., Scanes, P. R., Hudson, J.P., Nichol, S. L., 2001. Structure and function of south-east Australian estuaries. Estuarine, Coastal and Shelf Science 53, 351- 384.

Rustic, G.T., Koutavas, A., Marchitto, T.M., Linsley, B.K., 2015. Dynamical excitation of the tropical Pacific ocean and ENSO variability by Little ice age cooling. Science 350, 1537-1541.

Rustomji, P., Bennett, N., Chiew, F.H.S., 2009. Flood variability east of Australia's Great Dividing Range. J Hydrol. 375(304), 196-208.

Sachs, J.P., Sachse, D., Smittenberg, R.H., Zhang, Z.H., Battisti, D.S., Golubic, S., 2009. Southward movement of the Pacific intertropical convergence zone AD 1400-1850. Nature Geosci. 2(7), 519–525.

Saunders, K.M., Kamenik, C., Hodgson, D.A., Hunziker, S., Siffert, L., Fischer, D., Fujak, M., Gibson, J.A.E., Grosjean, M. 2012. Late Holocene changes in precipitation in northwest Tasmania and their potential links to shifts in the Southern Hemisphere westerly winds. Glob. Planet. Change 92 93, 82-91.

SEQ Water. 2013. Final Report January (Australia Day) 2013 weather event. p. 49.

Taylor, F., McMinn, A., 2001. Evidence from diatoms for Holocene climate fluctuation along the east Antarctic margin. The Holocene 11(4), 455-466.

Thompson, C.J., Croke, J.C. 2013. Geomorphic effects, flood power and channel competence of a catastrophic flood in confined and unconfined reaches of the upper Lockyer valley, south east Queensland, Australia. Geomorphology 197, 156-169.

Thompson, C.J., Croke, J.C., Grove, J.R., Khanal, G. 2013. Spatio-temporal changes in riverbank mass failures in the Lockyer valley, Queensland, Australia. Geomorphology 191, 129-141.

Thornton, S.F., McManus, J. 1994. Application of organic carbon and nitrogen stable isotope and C/N ratios as source indicators of organic matter provenance in estuarine systems: evidence from the Tay estuary, Scotland. Estuarine, Coastal and Shelf Science 38, 219-33.

Tibby, J. Reid, M. A. 2004. A model for inferring past conductivity in low salinity water derived from Murray River (Australia) diatom plankton. Marine and Freshwater Research 55, 597-607.

Tibby, J., Taffs, K. 2011. Palaeolimnology in eastern and southern Australian estuaries. Journal of Paleolimnology 46 (4), 503-510.

Ulm, S.F., Petchey, Ross, A., 2009. Marine reservoir corrections for Moreton Bay, Australia. Archaeology in Oceania 43 (3), 160-166.

van Dijk, A. J. M., Beck, H. E., Crosbie, R. S., de Jeu, R.A.M., Liu, Y.Y., Podger, G.M. Timbal, B., Viney, N. R. 2013 The millennium drought in southeast Australia (2001-2009): Natural and human causes and implications for water resources, ecosystems, economy and society. Water resource research 49 (2), 1040-1057.

Vance T.R., Roberts J.L., Plummer C.T. Kiem, A.S., van Ommen, T.D. 2015. Interdecadal Pacific variability and eastern Australian megadroughts over the last millennium. Geophysical Research Letters 42, 129-137.

Witkowski. A., Lange-Bertalot, H. and Metzeltin, D. 2001. Diatom Flora of Marine Coasts 1. Iconographia Diatomologica, Volume 7. A.R.G. Gantner Verlag, Ruggell, 925 pp.

Ward, P. J., Jongman, B., Kummu, M., Dettinger, M. D., Sperna Weiland, F. C., Winsemius, H. C. 2014. Strong influcnce of El Nino Southern Oscillation on flood risk around the world. PNAS 111 (44), 15659-15664.

Yan, H., Sun, L., Wang, Y., Huang, W., Qiu, S., Yang, C., 2011. A record of the Southern Oscillation Index for the past 2,000 years from precipitation proxies. Nat. Geosci. 4, 611-614.

Yi, S.H., Saito, Y., Oshima, H., Zhou, Y.Q. and Wei, H.L. 2003. Holocene environmental history inferred from pollen assemblagesin the Huanghe (Yellow River) Delta, China: climatic changes and human impact. Quaternary Science 22, 609-28.

Zong, Y., Lloyd, J.M., Leng, M.J., Yim, W.W.-S., Huang, G., 2006. The reconstruction of Holocene monsoon history from the Pearl River Estuary, using diatoms and carbon isotope ratios. The Holocene 16 (2), 251-263.

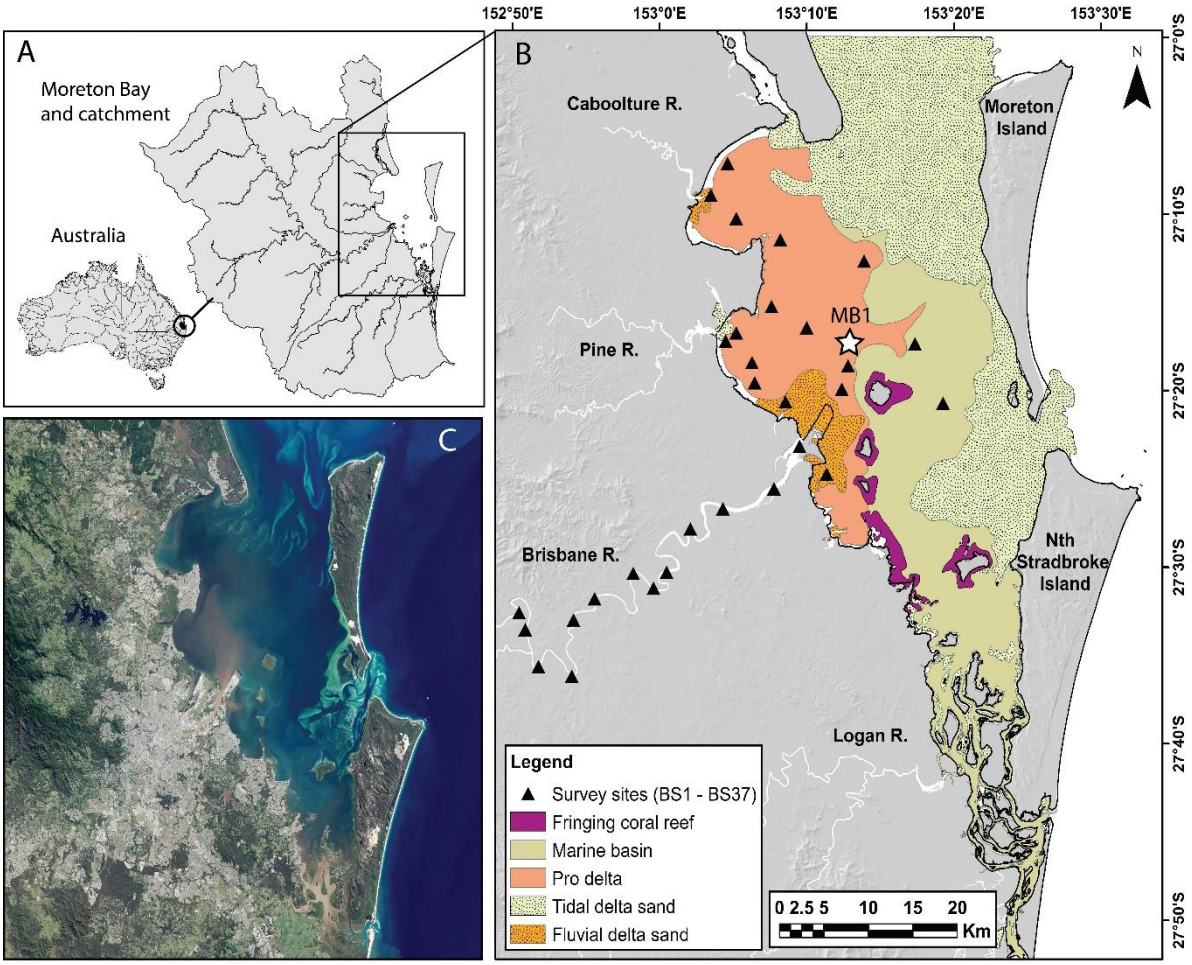

Figure 1. A) Moreton Bay and catchment detailing. B) Moreton Bay detailing major rivers draining into the Bay, (Caboolture, Pine Brisbane and Logan), islands (Moreton Is., North Stradbroke Is.), major subtidal sedimentary features mapped by Day *et al.*, 1983 (fluvial delta sand, marine basin, pro delta, tidal delta sand, fringing coral reef), and sampling locations of bottom sediments within the Brisbane River and Moreton Bay (BS 1- 37). Core site location MB1 is also indicated by the star. Background image source: DNRM, 2016. C) True colour LANDSAT 5 image of the Moreton Bay region after a minor flood event (May 2015) c)

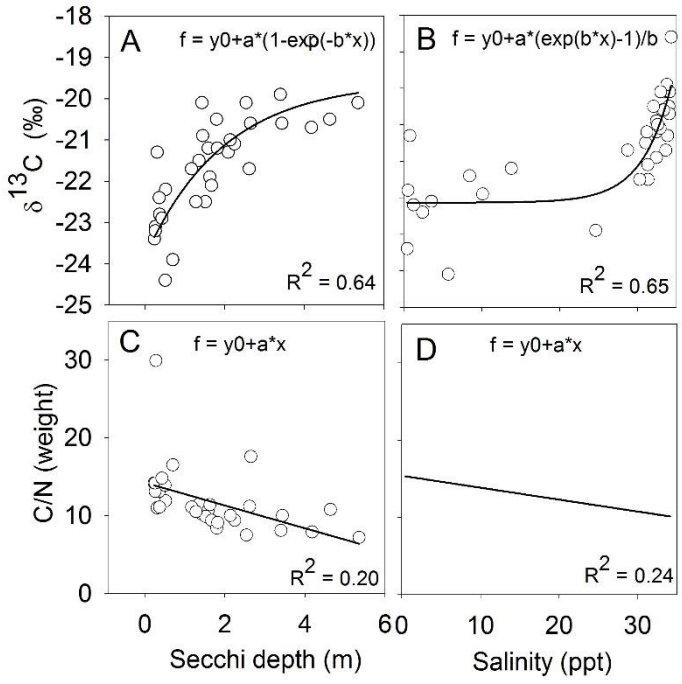

Figure 2. A) $\delta^{13}C$ versus secchi depth B)) $\delta^{13}C$ versus salinity. C) C/N versus secchi depth. D) C/N versus salinity.

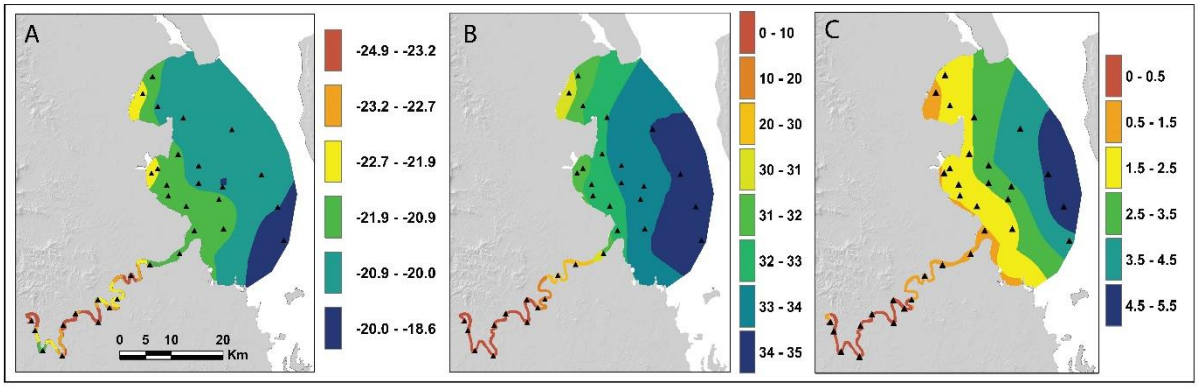

Figure 3. Contour plots of A) $\delta^{13}C$ ratios (‰) of bottom sediments. B) average salinity (ppt). C) secchi depth (m).

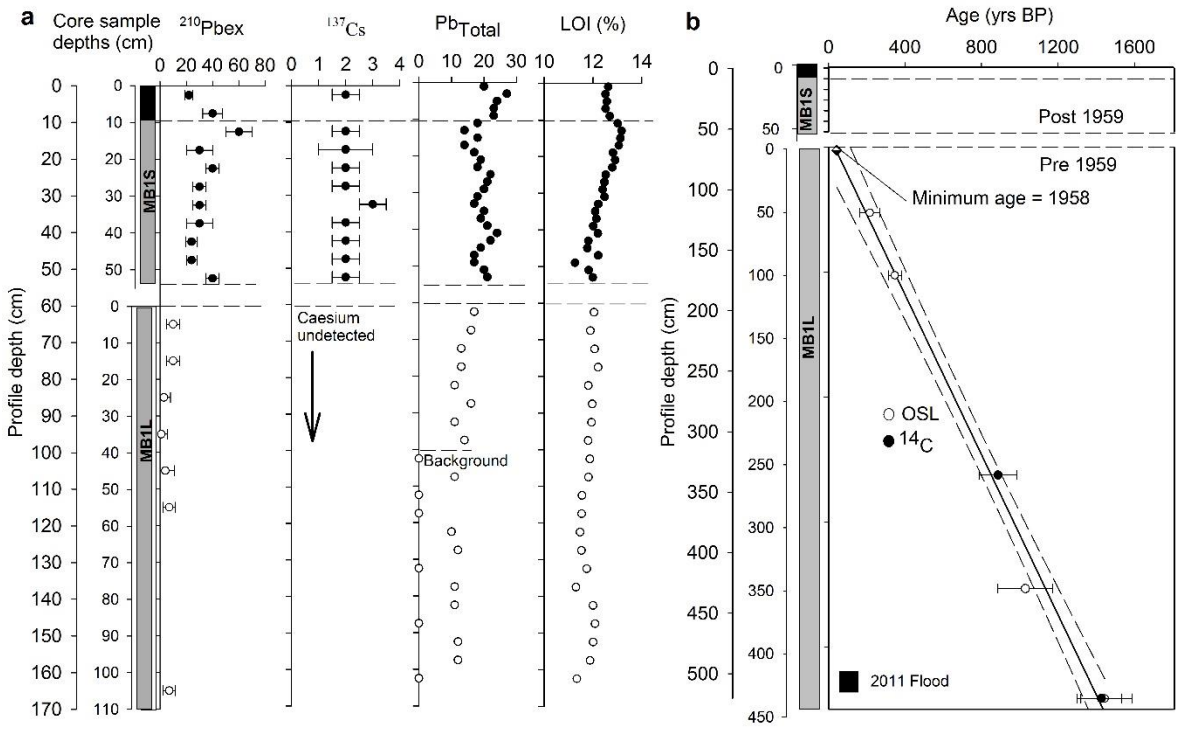

Figure 4. Summary of chronology at site MB1. Detailing OSL burial ages, AMS ^{14}C dates and the linear age (showing 95 % confidence interval) model for sediments deposited between ~600 to ~1959 CE. ^{137}Cs is used to define the post 1959 boundary with a linear age model used to define ages of samples between 1959 and 2010.

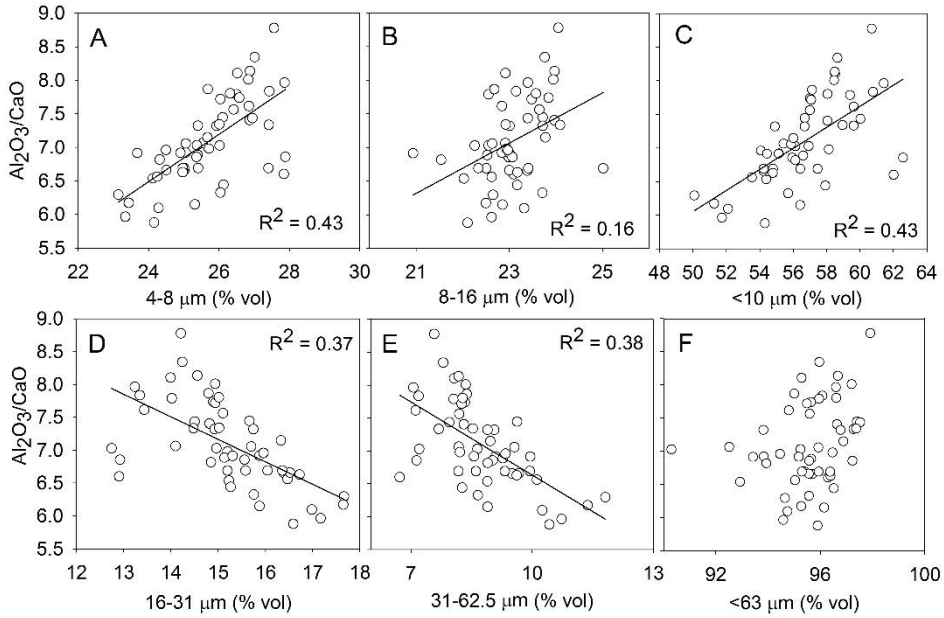

Figure 5. Relationship between major geochemistry (Al_2O_3/CaO) and grain size fractions measured for equivalent samples in the sediment profile at site MB1. A) Al_2O_3/CaO versus 4-8 µm. B) Al_2O_3/CaO versus 8-16 µm. C) Al_2O_3/CaO versus <10 µm. D) Al_2O_3/CaO versus 16-31 µm. E) Al_2O_3/CaO versus 31-62 µm. F) Al_2O_3/CaO versus <63 µm.

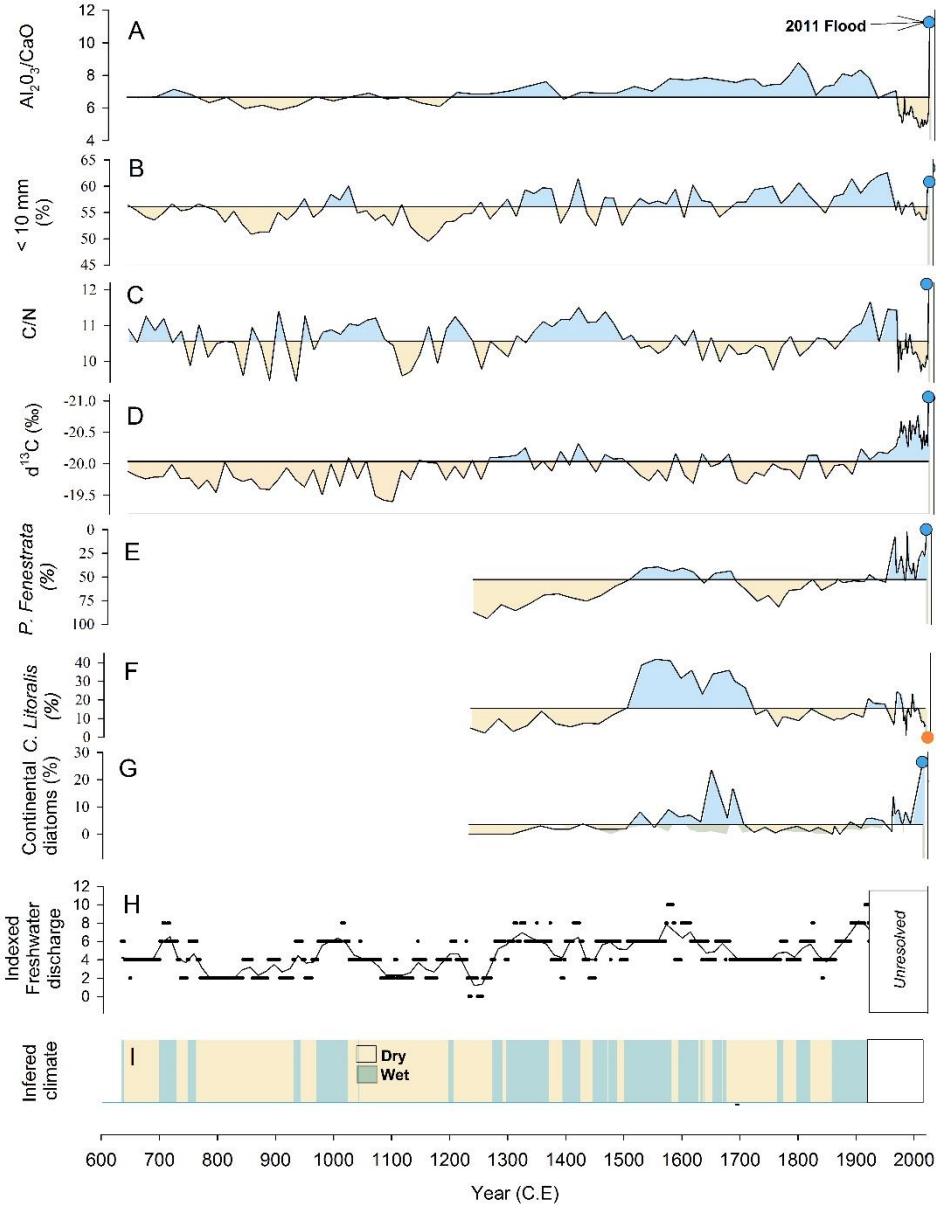

Figure 6. The multi-proxy record of freshwater influence in Moreton Bay for the last ~1500 years. Proxies of terrestrial input are presented on the y axis including; A) Al_2O_3/CaO, B) grain size (< 10 µm %). C) C/N ratios D) $\delta^{13}C$ ratios. E) *P. fenestrate* (%) F) *C. litoralis* G) Continental diatoms. The integrated record of freshwater input (indexed freshwater discharge (H)) including a moving average showing high and low periods associated with inferred wet and dry climates are also depicted (inferred climate (I)).

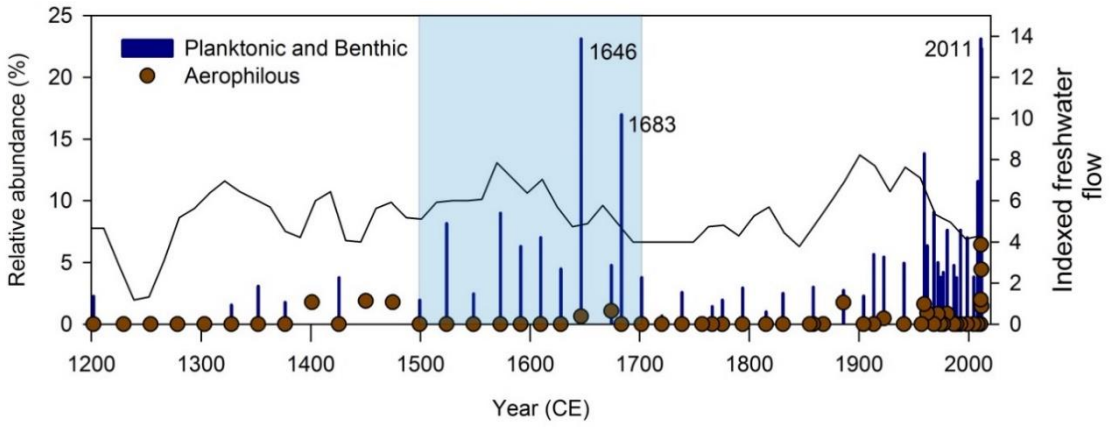

Figure 7. Continental diatom abundance from 1200 to 2011 including total planktonic and benthic, and aerophilous forms. The indexed freshwater flow is also shown.

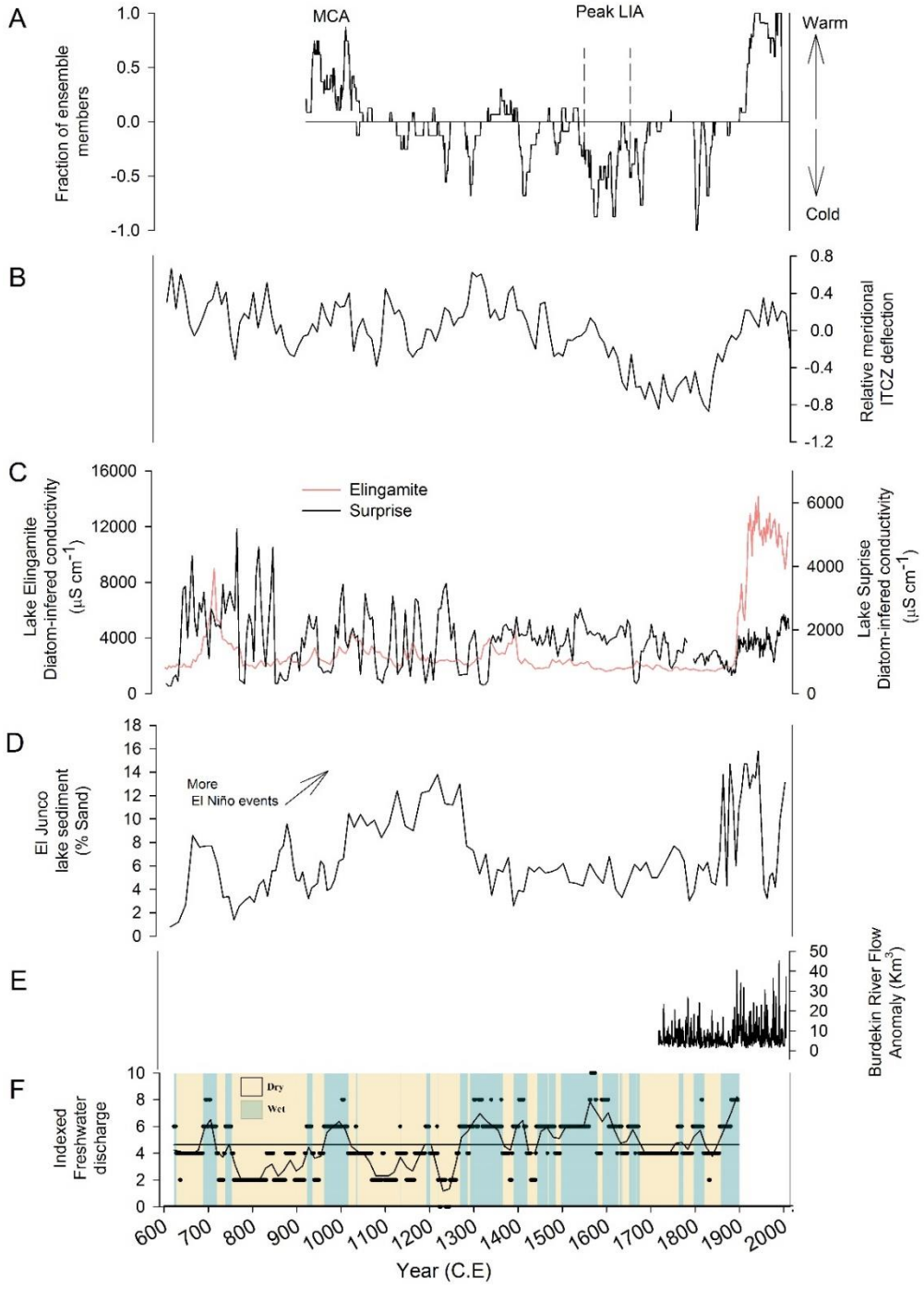

Figure 8. Comparison with regional climate records. A) Southern Hemisphere temperature anomalies (Neukom et al., 2014). B) Relative deflection of the ITCZ (-ive = southward, +ve = northward) (Lechleitner et al., 2017). C) Diatom-inferred trends in salinity of Lake Elingamite and Surprise in southern Australia (Barr et al., 2014). D) El Junco lake sediment % sand (Conroy et al., 2008). E) Freshwater discharge into the GBR Lagoon (Lough et al., 2015). F) Indexed freshwater flow and inferred climate (this study)

Table 1. Pearson's r values of bivariate correlations for $\delta^{13}C$, C/N and major water quality attributes^

	Chl *a* (mg/L)	Sal (ppt)	Secchi (m)	TN (mg/L)	TP (mg/Kg)	DO (%)	pH	Temp (C)	Turbidity (STU)
δ13C	-0.377*	0.720**	0.757**	-0.708**	-0.693	0.009	0.712**	-0.759**	-0.671**
C/N	-0.081	-0.352*	-0.399*	0.388*	0.389*	0.098	-0.395*	0.462**	0.401*

*p = < 0.005, ** p = < 0.001

^ Outliers excluded

Table 2. Age estimates of deposited sediment based on OSL and AMS ^{14}C dating

a) OSL burial ages and associated measurements including; saturated water content (Θ_s), burial dose (D_b) and dose rate (D_r).

Sample Code	Θ_s (%)	D_b (1σ)	D_r (1σ)	Burial age (Cal. yrs before 2011) (1σ).
MB1L 50_55	91	0.31 (0.07)	1.41 (0.12)	215 (51)
MB1L 100_105	87	0.52 (0.01)	1.49 (0.13)	346 (34)
MB1L 351_356	85	1.76 (0.16)	1.70 (0.18)	1029 (144)
MB1L 439_444	81	2.2 (0.07)	1.52 (0.14)	1444 (143)

b) Calibrated radiocarbon ages of shell material at given depths within MB1L

Sample Code	Lab code (BETA)	Material	Calibrated age* (Cal. yrs before 2011) (1σ)
MB1L 260_265	394745	Shell	885 (100)
MB1L 439_444	394746	Shell	1427 (107)

* Calibrated using MARINE13 and corrected for regional reservoir effect (ΔR = -219±94) (Ulm et al., 2009).